To appear in *Molecular Physics*
Vol. 00, No. 00, Month 2018, 1–18

RESEARCH ARTICLE

Kohn–Sham energy decomposition for molecules in a magnetic field

Sarah Reimann[a], Alex Borgoo[a], Jon Austad[a], Erik I. Tellgren[a], Andrew M. Teale[abc], Trygve Helgaker[bc], Stella Stopkowicz[db]

[a] *Department of Chemistry, Hylleraas Centre for Quantum Molecular Sciences, University of Oslo, P.O. Box 1033, Blindern, Oslo N-0315, Norway*;
[b] *Centre for Advanced Study at the Norwegian Academy of Science and Letters, Drammensveien 78, Oslo N-0271, Norway*;
[c] *School of Chemistry, University of Nottingham, University Park, Nottingham, NG7 2RD, UK*;
[d] Institut für Physikalische Chemie, Universität Mainz, Mainz D-55099, Germany

(*Received 00 Month 200x; final version received 00 Month 200x*)

We study the total molecular electronic energy and its Kohn–Sham components within the framework of magnetic-field density-functional theory (BDFT), an alternative to current-dependent density-functional theory (CDFT) for molecules in the presence of magnetic fields. For a selection of closed-shell dia- and paramagnetic molecules, we investigate the dependence of the total electronic energy and its Kohn–Sham components on the magnetic field. Results obtained from commonly used density-functional approximations are compared with those obtained from Lieb optimizations based on magnetic-field dependent relaxed coupled-cluster singles-and-doubles (CCSD) and second-order Møller–Plesset (MP2) densities. We show that popular approximate exchange–correlation functionals at the generalized-gradient-approximation (GGA), meta-GGA, and hybrid levels of theory provide a good qualitative description of the electronic energy and its Kohn–Sham components in a magnetic field—in particular, for the diamagnetic molecules. The performance of Hartree–Fock theory, MP2 theory, CCSD theory and BDFT with different exchange–correlation functionals is compared with coupled-cluster singles-doubles-perturbative-triples (CCSD(T)) theory for the perpendicular component of the magnetizability. Generalizations of the TPSS meta-GGA functional to systems in a magnetic field work well—the cTPSS functional, in particular, with a current-corrected kinetic-energy density, performs excellently, providing an accurate and balanced treatment of dia- and paramagnetic systems and outperforming MP2 theory.

Keywords: electron correlation, density-functional theory, current density-functional theory, magnetic-field density-functional theory, coupled-cluster theory, molecular magnetic properties, strong magnetic fields

1. Introduction

Kohn–Sham density-functional theory (DFT) is the most widely used method in quantum chemistry today. Over the last thirty years, a large number of density-functional approximations (DFAs) have been developed, leading to a good balance between accuracy and computational cost of DFT for a broad range of chemical applications [1]. However, DFT for molecules in a magnetic field has received much

*Corresponding author. Email: ajborgoo@gmail.com

ISSN: 0026 96 8976 print/ISSN 1362 96 3028 online

DOI: 10.1080/0026897YYxxxxxxxx
http://www.informaworld.com

less attention. As a result, little is known about the universal density functional in the presence of a magnetic field and the behaviour of existing DFAs for molecular magnetic properties is not fully satisfactory.

There are two main approaches to DFT in a magnetic field. The best known approach is perhaps current-density-functional theory (CDFT), where the effects of the field are described by introducing a dependence on the current density into the universal density functional [2–5]. Alternatively, in magnetic-field DFT (BDFT), the effects of the field are described by introducing an explicit field dependence into the universal functional [6]. In Ref. [7], we presented a common framework for the two approaches, relating the density functionals of CDFT and BDFT and their Kohn–Sham decompositions to each other within the four-way correspondence of convex analysis, which was used further in Ref. [8]. Furthermore, comparisons of BDFT adiabatic-connection curves of H_2 and LiH calculated using some popular DFAs with accurate curves calculated using field-dependent implementations of full-configuration-interaction (FCI) theory [9] and coupled-cluster-doubles (CCD) theory [10, 11] indicated that the main deficiency of the DFAs is present already in the absence of a magnetic field.

In this work, we extend our study of BDFT to a broader range of molecules, including larger molecules and closed-shell paramagnetic molecules, taking advantage of recent field-dependent implementations of relaxed densities from second-order Møller–Plesset (MP2) perturbation theory [12] and coupled-cluster singles-and-doubles (CCSD) theory [10, 13]. We assess the quality of several DFAs by comparing the field dependence of the total electronic energy and its Kohn–Sham components with CCSD and MP2 theories. The weak-field regime is assessed by comparing magnetizabilities calculated at the coupled-cluster singles-doubles-perturbative-triples (CCSD(T)) level of theory with those obtained using approximate exchange–correlation functionals. We conclude by studying the field dependence of the BDFT universal density functional for fixed densities.

After a discussion of BDFT in Section 2, DFAs in Section 3, and computational details in Section 4, we present and discuss our results in Section 5. Concluding remarks and directions for future work are given in Section 6.

2. Magnetic-field density-functional theory

In the presence of a magnetic field $\mathbf{B}$ represented by a vector potential $\mathbf{A}$ such that

$$\mathbf{B} = \nabla \times \mathbf{A}, \tag{1}$$

the spin-free electronic Hamiltonian of an N-electron molecular system in an external scalar potential v is given by

$$H_\lambda(v, \mathbf{A}) = T(\mathbf{A}) + \lambda W + \sum_{i=1}^{N} v(\mathbf{r}_i), \tag{2}$$

where $T(\mathbf{A})$ and W are the kinetic-energy and two-electron repulsion operators, respectively:

$$T(\mathbf{A}) = \frac{1}{2} \sum_{i=1}^{N} |-\mathrm{i}\nabla_i + \mathbf{A}(\mathbf{r}_i)|^2 , \quad W = \sum_{i>j} r_{ij}^{-1}. \tag{3}$$

The two-electron operator is scaled by the interaction-strength parameter λ, which is equal to one for the physical interacting system and zero for the noninteracting system. The N-electron ground-state energy is obtained from the Rayleigh–Ritz variation principle

$$E_\lambda(v,\mathbf{B}) = \inf_\gamma \operatorname{tr}\gamma H_\lambda(v,\mathbf{A}), \tag{4}$$

where the minimization is over N-electron ensemble states γ—that is, over convex combinations of pure N-electron states $|\Psi_i\rangle\langle\Psi_i|$ of a finite kinetic energy:

$$\gamma = \sum_i c_i|\Psi_i\rangle\langle\Psi_i|, \quad c_i \geq 0, \quad \sum_i c_i = 1. \tag{5}$$

The Hamiltonian $H_\lambda(v,\mathbf{A})$ in Eq. (2) is not uniquely defined since the magnetic field $\mathbf{B}$ determines the vector potential $\mathbf{A}$ only up to a gauge transformation. Nevertheless, the ground-state energy $E_\lambda(v,\mathbf{B})$ in Eq. (4) is well defined since, for each expectation value $\operatorname{tr}\gamma H_\lambda(v,\mathbf{A})$, a gauge transformation $\mathbf{A}\to\mathbf{A}'$ is precisely compensated for by a gauge transformation $\gamma\to\gamma'$ such that $\operatorname{tr}\gamma' H_\lambda(v,\mathbf{A}') = \operatorname{tr}\gamma H_\lambda(v,\mathbf{A})$. We do not attempt to characterize the set of admissible potentials v in Eq. (4) but note that the ground-state energy is well defined as an infimum even in those cases where a ground state (i.e., a minimizer) does not exist.

The ground-state energy $E_\lambda(v,\mathbf{B})$ is concave and continuous in v for a fixed $\mathbf{B}$. It can therefore be represented by a density functional $F_\lambda(\rho,\mathbf{B})$ that is convex in ρ for fixed $\mathbf{B}$ in the manner [6, 7]

$$E_\lambda(v,\mathbf{B}) = \inf_\rho \left[F_\lambda(\rho,\mathbf{B}) + (v|\rho)\right], \tag{6}$$

$$F_\lambda(\rho,\mathbf{B}) = \sup_v \left[E_\lambda(v,\mathbf{B}) - (v|\rho)\right], \tag{7}$$

where $(v|\rho) = \int v(\mathbf{r})\rho(\mathbf{r})\mathrm{d}\mathbf{r}$. In the following, we refer to Eqs. (6) and (7) as the Hohenberg–Kohn and Lieb variation principles, respectively. Alternatively, the density functional may be expressed in the constrained-search manner

$$F_\lambda(\rho,\mathbf{B}) = \inf_{\gamma\mapsto\rho} \operatorname{tr}\gamma H_\lambda(0,\mathbf{A}) \tag{8}$$

where a minimizer has been proven to exist for $\mathbf{A}=\mathbf{0}$ [14]. Note that the BDFT universal density functional is gauge invariant, depending on $\mathbf{B}$ rather than $\mathbf{A}$.

Assuming that a minimizer $\gamma_\lambda^{\rho,\mathbf{A}}$ exists for all $\lambda\in[0,1]$ in Eq. (8), we establish in the usual manner the adiabatic connection

$$F_\lambda(\rho,\mathbf{B}) = T_\mathrm{s}(\rho,\mathbf{B}) + \int_0^\lambda \mathcal{W}_\mu(\rho,\mathbf{B})\,\mathrm{d}\mu, \tag{9}$$

where $T_\mathrm{s}(\rho,\mathbf{B})$ is the non-interacting (mechanical) kinetic energy and $\mathcal{W}_\mu(\rho,\mathbf{B})$ the adiabatic-connection integrand in the presence of a magnetic field,

$$T_\mathrm{s}(\rho,\mathbf{B}) = F_0(\rho,\mathbf{B}) = \operatorname{tr}\gamma_0^{\rho,\mathbf{A}} T(\mathbf{A}), \tag{10}$$

$$\mathcal{W}_\lambda(\rho,\mathbf{B}) = F'_\lambda(\rho,\mathbf{B}) = \operatorname{tr}\gamma_\lambda^{\rho,\mathbf{A}} W. \tag{11}$$

Both quantities depend explicitly on $\mathbf{B}$ rather than $\mathbf{A}$ and are therefore gauge invariant. Introducing in the usual manner the Hartree functional J, the exchange

functional E_{x}, and the correlation functional E_{c},

$$J(\rho) = \iint \rho(\mathbf{r}_1)\rho(\mathbf{r}_2) r_{12}^{-1} \mathrm{d}\mathbf{r}_1 \mathrm{d}\mathbf{r}_2, \tag{12}$$

$$E_{\mathrm{x}}(\rho, \mathbf{B}) = \mathcal{W}_0(\rho, \mathbf{B}) - J(\rho), \tag{13}$$

$$E_{\mathrm{c},\lambda}(\rho, \mathbf{B}) = \int_0^\lambda \mathcal{W}_\mu(\rho, \mathbf{B}) \mathrm{d}\mu - \lambda E_{\mathrm{x}}(\rho, \mathbf{B}) - \lambda J(\rho) \tag{14}$$

we arrive at the Kohn–Sham decomposition of the BDFT universal density functional

$$F_\lambda(\rho, \mathbf{B}) = T_{\mathrm{s}}(\rho, \mathbf{B}) + \lambda J(\rho) + \lambda E_{\mathrm{x}}(\rho, \mathbf{B}) + E_{\mathrm{c},\lambda}(\rho, \mathbf{B}), \tag{15}$$

where all terms are gauge invariant. Often, the exchange and correlation functionals are combined into a single field-dependent exchange–correlation functional $E_{\mathrm{xc},\lambda}(\rho, \mathbf{B}) = \lambda E_{\mathrm{x}}(\rho, \mathbf{B}) + E_{\mathrm{c},\lambda}(\rho, \mathbf{B})$. While many approximations to the field-free exchange–correlation functional have been developed over the years, there have been only a few attempts at modelling its field dependence, mostly based on the original work by Vignale and coworkers [2, 15]. However, none of these functionals have proved successful for molecular properties [16–18].

Substituting the Kohn–Sham-decomposed density functional Eq.(15) into the Hohenberg–Kohn variation principle and assuming that a minimizing ground-state density ρ exists for the scalar potential v and magnetic field $\mathbf{B}$, we obtain the Kohn–Sham decomposition of the ground-state energy

$$E_\lambda(v, \mathbf{B}) = T_{\mathrm{s}}(\rho, \mathbf{B}) + (v|\rho) + \lambda J(\rho) + \lambda E_{\mathrm{x}}(\rho, \mathbf{B}) + E_{\mathrm{c},\lambda}(\rho, \mathbf{B}) \tag{16}$$

where again each term is gauge invariant.

We do not treat CDFT in detail here, referring instead to Refs. [2–4, 7, 8] for CDFT and its connection to BDFT. However, we note that the reparametrized energy functional [4]

$$\mathcal{E}_\lambda(u, \mathbf{A}) = E_\lambda(u - \tfrac{1}{2}A^2, \mathbf{A}) \tag{17}$$

is concave in both variables, unlike $E_\lambda(v, \mathbf{A})$, which is concave only in v. Invoking the theory of convex conjugation, we may then establish the CDFT Hohenberg–Kohn and Lieb variation principles in the usual manner

$$\mathcal{E}_\lambda(u, \mathbf{A}) = \inf_{\rho, \mathbf{j}_{\mathrm{p}}} \left[\mathcal{G}_\lambda(\rho, \mathbf{j}_{\mathrm{p}}) + (u|\rho) + (\mathbf{A}|\mathbf{j}_{\mathrm{p}})\right], \tag{18}$$

$$\mathcal{G}_\lambda(\rho, \mathbf{j}_{\mathrm{p}}) = \sup_{u, \mathbf{A}} \left[\mathcal{E}_\lambda(u, \mathbf{A}) - (u|\rho) - (\mathbf{A}|\mathbf{j}_{\mathrm{p}})\right], \tag{19}$$

where the CDFT density functional $\mathcal{G}_\lambda(\rho, \mathbf{j}_{\mathrm{p}})$ is convex in both the density ρ and the paramagnetic current density $\mathbf{j}_{\mathrm{p}}$.

3. Density-functional approximations

In this study, we compare accurate results obtained using the CCSD and MP2 models with results obtained using DFAs from four rungs of Jacob's ladder: the SVWN5 local density approximation (LDA), the PBE and BLYP generalized-

gradient-approximation (GGA) functionals, the B3LYP hybrid functional, and the TPSS meta-GGA (mGGA) functional.

3.1. *meta-GGA functionals in a magnetic field*

Given that meta-GGA functionals depend on the kinetic-energy density, we must ensure gauge invariance in the presence of a magnetic field. Following Maximoff and Scuseria [19], we work with the physical (mechanical) kinetic-energy density τ_{MS} to ensure gauge invariance

$$\tau_{\mathrm{MS}}(\mathbf{r}) = \frac{1}{2}\sum_{i=1}^{n_{\mathrm{occ}}} |\boldsymbol{\pi}\phi_i(\mathbf{r})|^2\,, \quad \boldsymbol{\pi} = -\mathrm{i}\boldsymbol{\nabla} + \mathbf{A}, \tag{20}$$

where $\boldsymbol{\pi}$ is the mechanical momentum operator. Since τ_{MS} depends explicitly on the vector potential and therefore on the magnetic field, this approach is well suited to BDFT. An alternative generalization of the kinetic-energy density to systems in a magnetic field, suited to CDFT, was proposed by Dobson [20],

$$\tau_{\mathrm{D}}(\mathbf{r}) = \tau_{\mathrm{can}}(\mathbf{r}) - \frac{\mathbf{j}_{\mathrm{p}}^2(\mathbf{r})}{2\rho(\mathbf{r})}, \tag{21}$$

with the canonical kinetic-energy density $\tau_{\mathrm{can}}(\mathbf{r}) = \frac{1}{2}\sum_{i=1}^{n_{\mathrm{occ}}} |\mathbf{p}\phi_i(\mathbf{r})|^2$ and the canonical momentum $\mathbf{p} = -\mathrm{i}\boldsymbol{\nabla}$. The τ_{MS} and τ_{D} functionals are both valid gauge-invariant generalizations of the field-free kinetic-energy density to systems with a magnetic field. However, when used with the TPSS meta-GGA functional, only τ_{D} extends the iso-orbital indicator of the field-free functional in a rigorous way [21]. In this work, we denote results obtained with the kinetic-energy density Eq. (20) and the TPSS functional by aTPSS, whilst those obtained with the kinetic-energy density Eq. (21) are denoted by cTPSS. This definition of cTPSS is the same as that introduced by Bates and Furche in Ref. [22], and calculations using this form have also been performed for atoms in strong magnetic fields previously by Zhu, Zhang and Trickey [23]. For further details on the implementation of DFT in a non-perturbative manner with London atomic orbitals, see Refs. [5, 18].

3.2. *meta-GGA Kohn–Sham matrix elements*

When evaluating the Kohn–Sham matrix contributions for the aTPSS and cTPSS functionals, we follow the standard practice of using derivatives of the exchange–correlation functional with respect to the one-particle reduced density matrix. This procedure avoids complexities associated with evaluating optimized effective potentials [24, 25] and yields non-multiplicative, orbital specific potentials. This 'functional-derivatives-with-respect-to-orbitals' (FDO) approach [26] is common practice for meta-GGA functionals.

We first express the quantities entering Eqs. (20) and (21) in the atomic-orbital basis as

$$\tau_{\mathrm{MS}}(\mathbf{r}) = \tfrac{1}{2}\sum\nolimits_{ba} (\boldsymbol{\pi}\chi_b(\mathbf{r})) \cdot D_{ba} (\boldsymbol{\pi}\chi_b(\mathbf{r}))^*, \tag{22}$$

$$\tau_{\mathrm{can}}(\mathbf{r}) = \tfrac{1}{2}\sum\nolimits_{ba} (\mathbf{p}\chi_b(\mathbf{r})) \cdot D_{ba} (\mathbf{p}\chi_a(\mathbf{r}))^*, \tag{23}$$

and

$$\rho(\mathbf{r}) = \sum\nolimits_{ab} \chi_b(\mathbf{r}) D_{ab} \chi_a^*(\mathbf{r}), \quad \mathbf{j}_\mathrm{p}(\mathbf{r}) = \tfrac{\mathrm{i}}{2} \sum\nolimits_{ab} \chi_b(\mathbf{r}) D_{ab} \nabla \chi_a^*(\mathbf{r}) + \text{c.c.} \tag{24}$$

where χ_a are the complex London atomic orbitals and the D_{ba} elements of the density matrix. Introducing the aTPSS and cTPSS exchange–correlation potentials

$$v_\mathrm{xc}^\mathrm{a}(\mathbf{r}) = \frac{\delta F_\mathrm{xc}^\mathrm{a}(\tau_\mathrm{MS}, \rho)}{\delta \rho(\mathbf{r})}, \quad \eta_\mathrm{xc}^\mathrm{a} = \frac{\delta F_\mathrm{xc}^\mathrm{a}(\tau_\mathrm{MS}, \rho)}{\delta \tau_\mathrm{MS}(\mathbf{r})}, \tag{25}$$

$$v_\mathrm{xc}^\mathrm{c}(\mathbf{r}) = \frac{\delta F_\mathrm{xc}^\mathrm{c}(\tau_\mathrm{D}, \mathbf{j}_\mathrm{p}, \rho)}{\delta \rho(\mathbf{r})}, \quad \eta_\mathrm{xc}^\mathrm{c} = \frac{\delta F_\mathrm{xc}^\mathrm{c}(\tau_\mathrm{D}, \mathbf{j}_\mathrm{p}, \rho)}{\delta \tau_\mathrm{D}(\mathbf{r})}, \quad \mathbf{A}_\mathrm{xc}^\mathrm{c} = \frac{\delta F_\mathrm{xc}^\mathrm{c}(\tau_\mathrm{D}, \mathbf{j}_\mathrm{p}, \rho)}{\delta \mathbf{j}_\mathrm{p}(\mathbf{r})}, \tag{26}$$

where superscripts ‘a’ and ‘c’ denote aTPSS and cTPSS, respectively, we obtain the following contributions to the Kohn–Sham matrix for the two functionals:

$$\begin{aligned}(F_\mathrm{xc}^\mathrm{a})_{ab} &= \left(v_\mathrm{xc}^\mathrm{a} \left| \tfrac{\partial \rho}{\partial D_{ba}} \right.\right) + \left(\eta_\mathrm{xc}^\mathrm{a} \left| \tfrac{\partial \tau_\mathrm{MS}}{\partial D_{ba}} \right.\right) \\ &= \left\langle \chi_a \left| v_\mathrm{xc}^\mathrm{a} + \tfrac{1}{2}\boldsymbol{\pi} \cdot \eta_\mathrm{xc}^\mathrm{a} \boldsymbol{\pi} \right| \chi_b \right\rangle, \end{aligned} \tag{27}$$

$$\begin{aligned}(F_\mathrm{xc}^\mathrm{c})_{ab} &= \left(v_\mathrm{xc}^\mathrm{c} \left| \tfrac{\partial \rho}{\partial D_{ba}} \right.\right) + \left(\mathbf{A}_\mathrm{xc}^\mathrm{c} \left| \tfrac{\partial \mathbf{j}_\mathrm{p}}{\partial D_{ba}} \right.\right) + \left(\eta_\mathrm{xc}^\mathrm{c} \left| \tfrac{\partial \tau_\mathrm{can}}{\partial D_{ba}} \right.\right) \\ &= \left\langle \chi_a \left| v_\mathrm{xc}^\mathrm{c} + \tfrac{1}{2}\{\mathbf{p}, \mathbf{A}_\mathrm{xc}^\mathrm{c}\} + \tfrac{1}{2}\mathbf{p} \cdot \eta_\mathrm{xc}^\mathrm{c} \mathbf{p} \right| \chi_b \right\rangle. \end{aligned} \tag{28}$$

For the aTPSS functional, the term containing $\eta_\mathrm{xc}^\mathrm{a}$ can be decomposed as $\frac{1}{2}\boldsymbol{\pi} \cdot \eta_\mathrm{xc}^\mathrm{a} \boldsymbol{\pi} = \frac{1}{2}\mathbf{p} \cdot \eta_\mathrm{xc}^\mathrm{a} \mathbf{p} + \frac{1}{2}\{\mathbf{p}, \mathbf{A}\eta_\mathrm{xc}^\mathrm{a}\} + \frac{1}{2}\eta_\mathrm{xc}^\mathrm{a} A^2$, where $\mathbf{A}\eta_{xc}^\mathrm{a}$ is an effective vector potential that modifies terms linear in $\mathbf{p}$.

Two remarks are in order. First, our BDFT Kohn–Sham implementation is based on the use of London atomic orbitals with the external magnetic field $\mathbf{A}$ explicitly retained; see Eq. (8) of Ref. [6]. Hence, we do not attempt to further reduce the BDFT equations to a purely real form as proposed in Eq. (12) of Ref. [6]. Second, we note that the optimization of the aTPSS and cTPSS functionals with respect to the density matrix blurs the distinction between the BDFT and CDFT frameworks, since the functionals lacks a non-trivial dependence on either the external field or the vorticity—see Section 2.5 in Ref. [7] for further discussion.

4. Computational details

We have studied He, H_2, He_2, Be, H_2O, HF, Ne, N_2, CO, NH_3, BH, CH^+, AlH, BeH^-, and SiH^+ with CCSD theory and benzene C_6H_6 and pyrrole C_4H_5N with MP2 theory. All systems except BH, CH^+, SiH^+, and AlH are diamagnetic. BeH^- is a borderline case, being globally (slightly) diamagnetic, at least when treated at the coupled-cluster level, but it does have more pronounced paramagnetic components of the magnetizability perpendicular to the bond axis. For previous studies of these paramagnetic systems we refer the reader to work by Fowler and Steiner [27] and Sauer *et al.* [28].

For H_2 and He_2, we used bond lengths $1.4a_0$ and $5.7a_0$, respectively (approximate equilibrium distances). The CCSD(T)/cc-pVTZ geometries of H_2O, HF, N_2, CO, and NH_3 are taken from Refs. [29] and [30], whereas the cc-pVTZ+sp/RAS-MRCISD bond lengths of BH and CH^+ are from Ref. [31]. The AlH bond distance was optimized at the MP2/aug-cc-pVTZ level yielding $2.07982a_0$. For BeH^- and SiH^+, the geometries were optimized at the CCSD(T) level in the uncontracted Cartesian

aug-cc-pVTZ basis giving bond distances of $2.68283a_0$ and $2.85101a_0$, respectively. For benzene, we used CC and CH bond lengths of $2.6353a_0$ and $2.0504a_0$, respectively, corresponding to the optimized MP2/6-31G* geometry. For pyrrole, we used the MP2/cc-pVTZ geometry from Ref. [32].

All atomic and molecular calculations reported in this paper are for field strengths between 0 and about 7000 Tesla ($0 \leq B/B_0 \leq 0.03, 1B_0 \approx 235,000\,\mathrm{T}$). This range provides valuable information about the behaviour of energy components, while staying well below field strengths that induce level crossings in the fully interacting or non-interacting systems. Moreover, these field strengths can be studied confidently without the need for field-dependent, anisotropic basis sets [33]. The direction of the magnetic field vector was chosen perpendicular to the molecular axis or plane. In NH_3, the field is directed along the symmetry axis away from the nitrogen atom.

The reference data for the magnetizabilities at the HF, MP2, CCSD, and CCSD(T) levels of theory was generated using the `CFOUR` program package [34] as described in Ref. [35]. The density-functional calculations were performed using the `QUEST` program [36] and all other calculations were performed using the `LONDON` quantum-chemistry software [37, 38]. In all calculations, London atomic orbitals [39] were employed to ensure gauge-origin independence. Unless otherwise stated, we have used the uncontracted aug-cc-pVTZ basis of Dunning and coworkers [40, 41], denoted as unc-aug-cc-pVTZ, in Cartesian rather than spherical-harmonic form.

To obtain $T_\mathrm{s}(\rho, \mathbf{B})$ for the wave-function methods, we performed Lieb optimizations [7, 42, 43] at $\lambda = 0$ where the reference density ρ is a relaxed CCSD [13] or MP2 [12] density calculated with $\lambda = 1$ in the field $\mathbf{B}$. The Kohn–Sham components $J(\rho)$ and $(v|\rho)$ were obtained from the same CCSD (MP2) densities whereas $E_\mathrm{xc}(\rho, \mathbf{B})$ was obtained by subtracting $T_\mathrm{s}(\rho, \mathbf{B}) + J(\rho) + (v|\rho)$ from the CCSD (MP2) ground-state energy in Eq. (16) at $\lambda = 1$.

5. Results and discussion

In Section 5.1, we discuss the field dependence of the total energy and the Kohn–Sham components, comparing CCSD (MP2) curves with aTPSS curves. Next, in Section 5.2, we discuss magnetizabilities, comparing CCSD(T) values with other wave-function models and several DFAs. Finally, in Section 5.3, we examine the field dependence of the BDFT density functionals for a fixed density.

5.1. *Field dependence of the total energy and its Kohn–Sham components*

We consider diamagnetic atoms and molecules first, in Section 5.1.1, followed by a discussion of closed-shell paramagnetic molecules in Section 5.1.2.

5.1.1. Diamagnetic atoms and molecules

In Figure 1, the changes in the total electronic energy and its Kohn–Sham components are shown as functions of field strength relative to their respective zero-field values for the diamagnetic systems He, He_2, H_2, Be, NH_3, H_2O, HF, Ne, N_2, CO, C_6H_6 (benzene), and C_4H_5N (pyrrole). Each plot contains two sets of curves: the full lines correspond to MP2 theory for benzene and pyrrole and to CCSD theory for all other systems; the dotted lines correspond to BDFT with the aTPSS functional for all systems. No CCSD data is available for benzene and pyrrole but, for all other molecules, the MP2 curves (not shown here) are almost indistinguishable from the CCSD curves on the scale of the plots. For the two-electron systems He and H_2, the CCSD model corresponds to the FCI model.

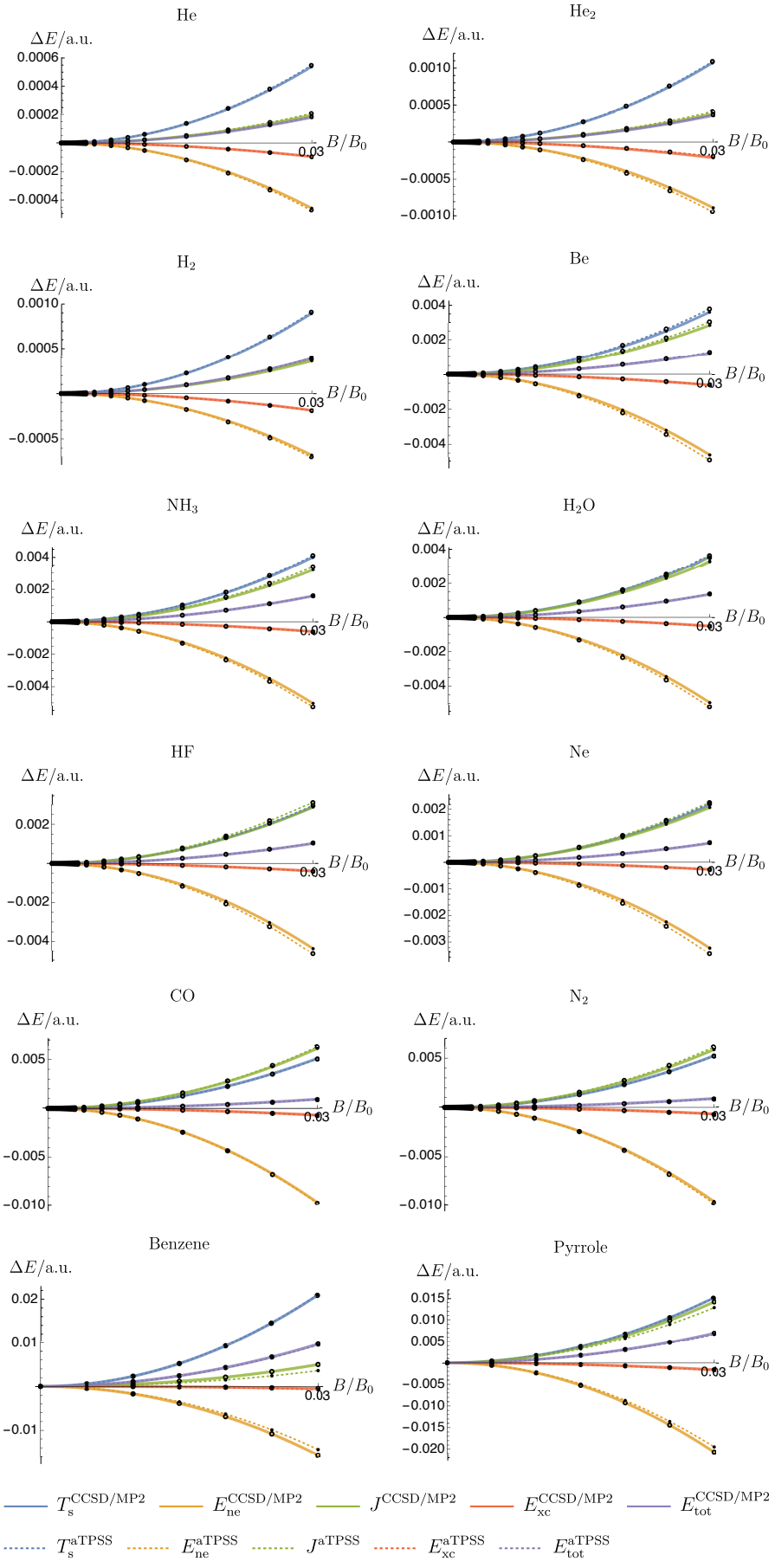

Figure 1. The total energy and Kohn–Sham components for diamagnetic atoms and molecules relative to their zero-field values as a function of the magnetic field strength. The full curves have been calculated using CCSD theory except for benzene and pyrrole, for which MP2 theory has been used. All calculations have been carried out with the unc-aug-cc-pVTZ basis, at zero-field equilibrium geometry in a perpendicular orientation to the field.

All diamagnetic systems show a similar characteristic behaviour. As the field is applied, the noninteracting kinetic energy $T_s(\rho, \mathbf{B})$ (blue curve) increases because of the induced precessional motion. At the same time, the applied field confines the charge density, giving a more negative nuclear-attraction energy $(v|\rho)$ (yellow curve), which is partly offset by an increase in the Hartree energy $J(\rho)$ (green curve). As a result, the total Coulomb energy $J(\rho) + (v|\rho)$ is lowered in the field. The exchange–correlation energy (red curve) also becomes more negative in the field but it is less affected than the other Kohn–Sham terms. Since all molecules in Figure 1 are diamagnetic, the total energy (purple curve) increases in all cases.

What differs considerably between the various systems in Figure 1 is the extent to which the increase in the kinetic energy is offset by the lowering of the total Coulomb energy. For many systems, the net increase in the electronic energy is about one half of the increase in the kinetic energy; for other systems, it is closer to one quarter (e.g., CO and N_2).

Bearing in mind the relatively small changes observed in the exchange–correlation energy in the magnetic field, we would expect DFAs to give a reasonably good description of the same systems in the field. Indeed, the behaviour of the aTPSS functional vis-a-vis CCSD/MP2 theory is good—for all systems, the field dependence of the total energy and its Kohn–Sham components is accurately reproduced by the aTPSS functional. All DFAs considered in this work (LDA, BLYP, B3LYP, aTPSS, and cTPSS) behave in a similar manner.

5.1.2. Paramagnetic molecules

Unlike for diamagnetic molecules, the electronic structure of closed-shell paramagnetic molecules undergoes dramatic changes when an external field is applied. As explained in Ref. [44], closed-shell paramagnetism arises when the zero-field ground state couples with low-lying excited states in the presence of the field, lowering the ground-state energy. The correct description of closed-shell paramagnetism is therefore a more difficult task than the correct description of closed-shell diamagnetism.

In Figure 2, we have plotted the changes in total electronic energy and its Kohn–Sham components against the magnetic field strength relative to their respective zero-field values for the closed-shell paramagnetic molecules BH, CH^+, and AlH. To the left, we compare the CCSD and MP2 curves; to the right, we compare CCSD and aTPSS curves. Unlike for the diamagnetic molecules, there are relatively large differences between the CCSD and MP2 curves and even larger differences between the CCSD and aTPSS curves—in particular, for AlH.

The behaviour of the neutral molecules BH and AlH in Figure 2 is opposite to that of the (neutral) diamagnetic molecules in Figure 1: the noninteracting kinetic energy and the Hartree energy decrease in the field, while the nuclear-attraction energy and the exchange–correlation energy increase. The CH^+ molecule behaves differently in that the lowering of the noninteracting kinetic energy in the field is accompanied by an increase in the Hartree energy and a decrease in the nuclear-attraction energy. This unexpected behaviour is perhaps related to the compact electronic structure of the positively charged CH^+ molecule.

Whereas the exchange–correlation energy of diamagnetic molecules is lowered slightly with increasing field strength, it increases strongly for all paramagnetic molecules, reflecting the dramatic changes that occur in paramagnetic molecules with the application of a field. Since the changes in the exchange–correlation energy are as large as or even larger than the changes in the total energy (but in the opposite direction), the performance of the DFAs for paramagnetic molecules varies more widely than for diamagnetic molecules.

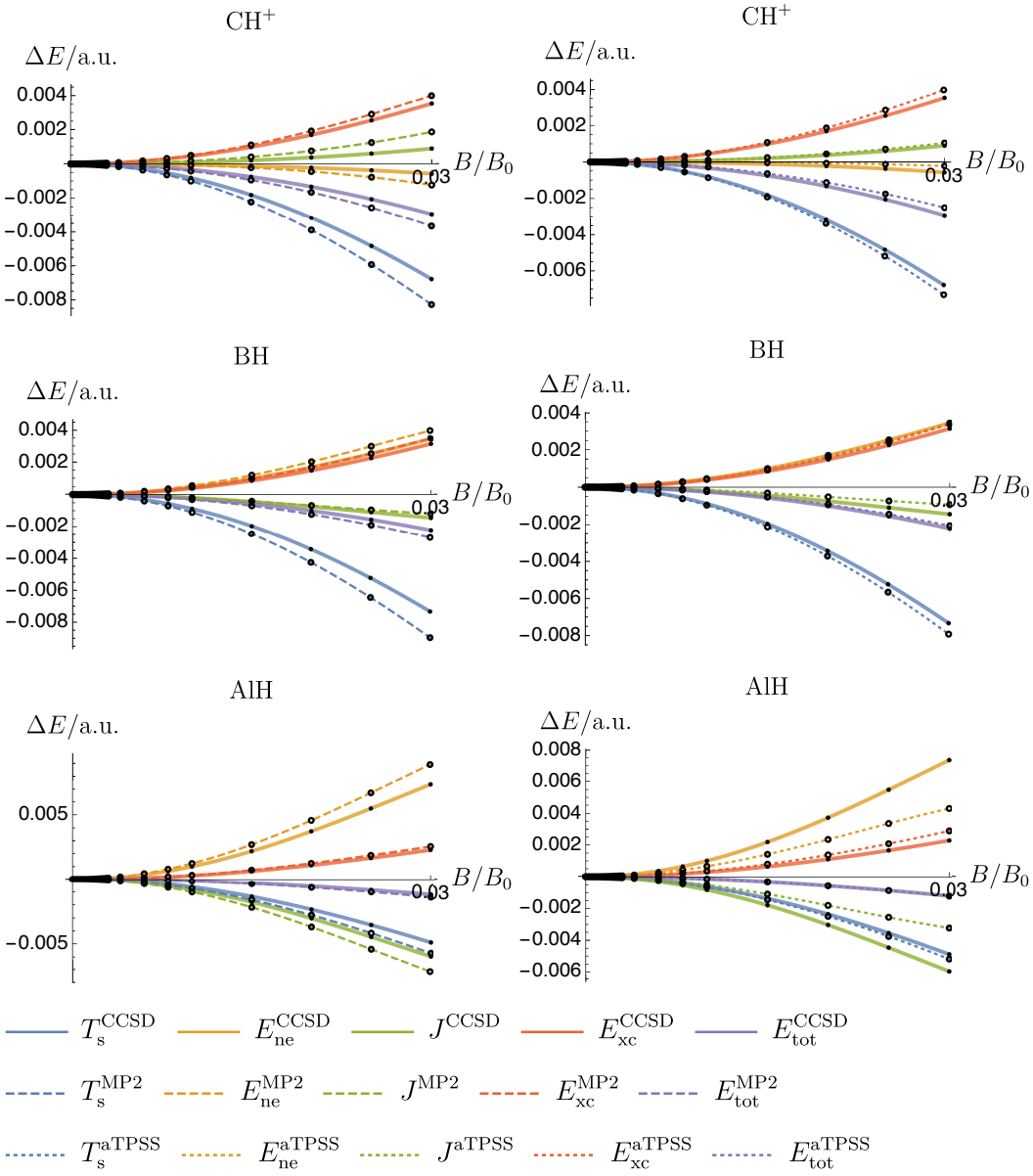

Figure 2. The total energy and its Kohn–Sham components for paramagnetic molecules relative to the zero-field values as a function of the magnetic field strength; CCSD and MP2 curves to the left; CCSD and aTPSS curves to the right. All calculations have been carried out with the unc-aug-cc-pVTZ basis, at zero-field equilibrium geometry in a perpendicular orientation to the field.

5.2. *Magnetizabilities*

The curves of the total energy and its Kohn–Sham components in Figures 1 and 2 show a quadratic dependence on the magnetic field strength. For the field strengths considered here, therefore, the field dependence of the total electronic energy should be accurately described by the magnetizability, which by definition is equal to minus the second derivative of the total energy with respect to the magnetic field at zero field. For a given electronic-structure method, we may then quantify the behaviour of the total energy and the Kohn–Sham components in the low-field regime (here up to about 7000 T) by examining the error in the calculated magnetizability.

The quality of calculated magnetizabilities has been subject of several studies before—particularly relevant are the coupled-cluster study of Gauss *et al.* from 2007 [35], the DFT and coupled-cluster benchmark study of Lutnæs *et al.* from

2009 [29], and the MP2 benchmark study of Loibl and Schütz from 2014 [45]. Our study differs from these by including paramagnetic as well as diamagnetic molecules and by considering meta-GGA functionals, recently identified as well suited to calculations in a magnetic field [5, 7].

Table 1 contains the magnetizabilities calculated at the Hartree–Fock (HF), all-electron MP2, CCSD, and CCSD(T) levels of theory in the unc-aug-cc-pVTZ and spherical-harmonic aug-cc-pCV5Z basis sets. The magnetizabilities of the diamagnetic molecules are reasonably well converged in the unc-aug-cc-pVTZ basis, the largest difference between the TZ and 5Z values being $0.4 \cdot 10^{-30}$ JT^{-2} for the HF model and $1.7 \cdot 10^{-30}$ JT^{-2} for the CCSD model. Correlation effects beyond the CCSD level are of the same order of magnitude and in most cases opposite in sign, leading to rather small errors between the magnetizabilities obtained at the CCSD/unc-aug-cc-pVTZ level as compared to the CCSD(T)/aug-cc-pCV5Z reference numbers (see column 'diff' in Table 1). For the paramagnetic molecules, the basis-set effects and the contribution from triple excitations are larger, leading to deviations of up to $17.2 \cdot 10^{-30}$ JT^{-2} (in the perpendicular component of SiH^+).

As discussed in Section 5.1.2, the perpendicular component of the magnetizability tensor, ξ_{xx}, is in general most sensitive to the correlation treatment and the basis-set quality. We therefore focus on this component in the following, assessing the errors of each method relative to the CCSD(T)/aug-cc-pCV5Z data in Table 1. We note that this magnetizability component corresponds to minus the second derivative at zero field of the curves plotted in Figures 1 and 2.

In Table 2, we have, for different models in the unc-aug-cc-pCVTZ basis, listed the mean error (ME), mean absolute error (MAE), mean percentage error (MPE), and mean absolute percentage error (MAPE) in the calculated ξ_{xx} relative to all-electron CCSD(T)/aug-cc-pCV5Z values. The same errors are illustrated in Figure 3. For the DFAs considered in this work, we have confirmed that use of the larger unc-aug-cc-pVQZ basis does not significantly affect the results; the largest differences are $0.2 \cdot 10^{-30}$ JT^{-2} and $3.8 \cdot 10^{-30}$ JT^{-2} for the dia- and paramagnetic molecules, respectively. Recalling the different behaviour for the dia- and paramagnetic molecules noted in Section 5.1, we have presented errors also separately for dia- and paramagnetic molecules in Table 2 and highlighted the data points corresponding to paramagnetic molecules by red circles in Figure 3.

From Table 2 and Figure 3, we see that the best overall performance is that of CCSD theory and the cTPSS functional, whereas LDA gives the poorest performance. The good performance of the cTPSS functional is striking: it is the only method that gives similar errors for the dia- and paramagnetic molecules—all other methods give errors that are one or two orders of magnitude larger for the paramagnetic molecules. The modest performance of MP2 theory is consistent with the observations by Loibl and Schütz [45]. Regarding the CCSD method, we observe that the basis-set and correlation errors are of the same order of magnitude.

Focusing on the diamagnetic molecules, we note that the mean absolute percentage errors range from 0.3% for the CCSD model to 4.5% for LDA. For the other DFAs, the mean absolute errors are 2.3% to 3.3%, compared with 2.3% and 1.8% for the HF and MP2 models, respectively. The CCSD model clearly performs best, with mean and mean absolute errors of $-0.3 \cdot 10^{-30}$ JT^{-2} and $0.4 \cdot 10^{-30}$ JT^{-2}, respectively, about one order of magnitude smaller than for the other methods.

Considering the paramagnetic molecules, the cTPSS functional gives a mean absolute percentage error of 1%, compared with 4.9% for CCSD. Errors for the other methods are an order of magnitude larger, the largest being 31.7% for LDA. Except for CCSD and aTPSS, all methods overestimate ξ_{xx} for these molecules.

Regarding the cTPSS functional, we have previously observed that it performs

Table 1. Total magnetizabilities and components (xx, yy, and zz, where the zz-component corresponds to the parallel orientation) in units of 10^{-30} J T^{-2}, calculated at the HF, MP2, CCSD, and CCSD(T) levels of theory in the Cartesian unc-aug-cc-pVTZ and contracted spherical aug-cc-pCV5Z basis sets.

		unc-aug-cc-pVTZ				aug-cc-pCV5Z				diff*
		HF	MP2	CCSD	CCSD(T)	HF	MP2	CCSD	CCSD(T)	
Diamagnetic molecules:										
He	total	-31.2	-31.3	-31.5	-	-31.2	-31.3	-31.4	-	0.0
Be	total	-227.8	-220.0	-214.3	-214.1	-227.8	-219.4	-214.0	-213.8	0.5
Ne	total	-123.4	-126.9	-126.0	-126.4	-123.3	-126.4	-125.5	-125.9	0.1
H_2	$xx = yy$	-69.2	-68.7	-68.5	-	-69.2	-68.6	-68.4	-	0.1
	zz	-61.4	-60.6	-60.3	-	-61.3	-60.4	-60.1	-	0.2
	total	-66.6	-66.0	-65.8	-	-66.6	-65.9	-65.6	-	0.2
He_2	$xx = yy$	-62.3	-62.6	-62.9	-62.9	-62.3	-62.5	-62.8	-62.8	0.1
	zz	-62.3	-62.7	-62.9	-62.9	-62.3	-62.6	-62.8	-62.8	0.1
	total	-62.3	-62.7	-62.9	-62.9	-62.3	-62.5	-62.8	-62.8	0.1
N_2	$xx = yy$	-151.8	-166.0	-159.5	-159.3	-151.6	-164.5	-158.4	-158.1	1.5
	zz	-304.9	-301.1	-301.3	-301.7	-304.9	-300.0	-300.3	-300.6	0.7
	total	-202.8	-211.0	-206.8	-206.8	-202.7	-209.7	-205.7	-205.6	1.2
CO	$xx = yy$	-157.1	-172.9	-166.2	-166.4	-156.6	-170.8	-164.4	-164.5	1.6
	zz	-300.0	-303.5	-301.3	-301.9	-299.8	-302.3	-300.0	-300.6	0.7
	total	-204.7	-216.4	-211.2	-211.5	-204.4	-214.6	-209.6	-209.9	1.3
HF	$xx = yy$	-175.6	-181.6	-179.4	-180.1	-175.5	-180.8	-178.5	-179.3	0.1
	zz	-166.9	-172.8	-170.8	-171.6	-166.8	-172.1	-170.0	-170.7	0.1
	total	-172.7	-178.7	-176.5	-177.3	-172.6	-177.9	-175.7	-176.5	0.1
H_2O	xx	-233.1	-240.1	-236.3	-237.3	-232.9	-239.1	-235.4	-236.4	-0.1
	yy	-228.9	-236.6	-233.1	-234.1	-228.7	-235.6	-232.0	-233.1	0.0
	zz	-231.8	-239.6	-236.0	-237.1	-232.0	-238.9	-235.2	-236.3	-0.3
	total	-231.3	-238.8	-235.1	-236.2	-231.2	-237.9	-234.2	-235.2	-0.1
CH_4	total	-313.9	-321.7	-317.0	-318.0	-313.6	-320.8	-316.2	-317.5	-0.5
NH_3	$xx = zz$	-293.1	-300.6	-295.9	-297.0	-292.9	-299.6	-294.9	-296.1	-0.2
	yy	-276.7	-284.0	-279.3	-280.3	-276.4	-283.0	-276.4	-279.4	-0.2
	total	-287.6	-295.1	-290.3	-291.5	-287.4	-294.0	-288.8	-290.5	-0.2
Paramagnetic molecules:										
BH	$xx = yy$	560.4	498.5	405.5	413.8	560.2	506.7	411.2	418.7	13.2
	zz	-198.2	-197.6	-196.2	-196.6	-198.1	-196.8	-195.6	-196.0	0.2
	total	307.5	266.5	204.9	210.4	307.4	272.2	208.9	213.8	8.8
CH^+	$xx = yy$	834.0	665.3	533.6	540.9	833.3	678.5	540.9	546.7	13.0
	zz	-113.9	-113.9	-113.8	-113.9	-113.8	-113.5	-113.4	-113.6	0.2
	total	518.0	405.6	317.8	322.6	517.6	414.5	322.8	326.6	8.8
AlH	$xx = yy$	282.6	270.1	229.0	237.2	277.3	273.1	233.5	239.8	10.7
	zz	-365.9	-363.2	-362.6	-363.2	-365.3	-358.2	-358.5	-358.9	3.7
	total	66.4	59.0	31.8	37.1	63.1	62.6	36.2	40.2	8.4
SiH^+	$xx = yy$	272.6	262.9	230.7	242.6	271.1	267.6	237.5	247.9	17.2
	zz	-249.0	-249.0	-249.0	-249.2	-248.7	-246.9	-247.0	-247.3	1.7
	total	98.7	92.2	70.8	78.6	97.8	96.1	76.0	82.9	12.0
BeH^-	$xx = yy$	328.3	301.5	231.1	247.9	321.6	297.8	229.7	246.8	15.7
	zz	-601.8	-594.6	-577.5	-580.2	-609.8	-602.3	-585.3	-588.4	-10.9
	total	18.3	2.8	-38.4	-28.1	11.1	-2.2	-42.0	-31.6	6.8

* Difference between magnetizabilities of our best estimate (CCSD(T)/aug-cc-pCV5Z) and CCSD/unc-aug-cc-pVTZ level of theory.

Table 2. Error measures for the perpendicular component of the magnetizability tensor, ξ_{xx} relative to the CCSD(T)/aug-cc-pCV5Z data, in units of 10^{-30} JT^{-2} for ME and MAE. All calculations have been carried out for the indicated method with the unc-aug-cc-pVTZ basis.

		HF	MP2	CCSD	cTPSS	aTPSS	B3LYP	BLYP	PBE	LDA
Total	ME	37.1	16.3	−4.6	0.4	−13.4	21.8	15.2	22.7	46.7
	MAE	38.9	21.1	4.7	3.7	15.3	24.3	19.2	26.4	53.8
	MPE	8.6	6.3	−1.3	−0.3	−2.7	7.1	6.6	8.0	16.5
	MAPE	8.4	5.6	1.7	1.9	5.6	6.9	6.4	8.0	13.0
Dia.	ME	1.4	−3.5	−0.3	1.2	−1.0	−0.7	−2.1	−1.1	−3.7
	MAE	4.1	3.5	0.4	3.5	3.8	2.9	3.6	4.3	6.5
	MPE	−0.9	1.8	0.2	−0.4	0.9	0.9	2.0	1.3	2.9
	MAPE	2.3	1.8	0.3	2.3	2.6	2.3	2.8	3.3	4.5
Para.	ME	115.6	59.7	−14.0	−1.4	−40.6	71.4	53.5	75.1	157.7
	MAE	115.6	59.7	14.0	4.1	40.6	71.4	53.5	75.1	157.7
	MPE	29.4	16.3	−4.7	−0.1	−10.6	20.7	16.8	22.8	46.6
	MAPE	21.8	13.8	4.9	1.0	12.4	17.1	14.3	18.4	31.7

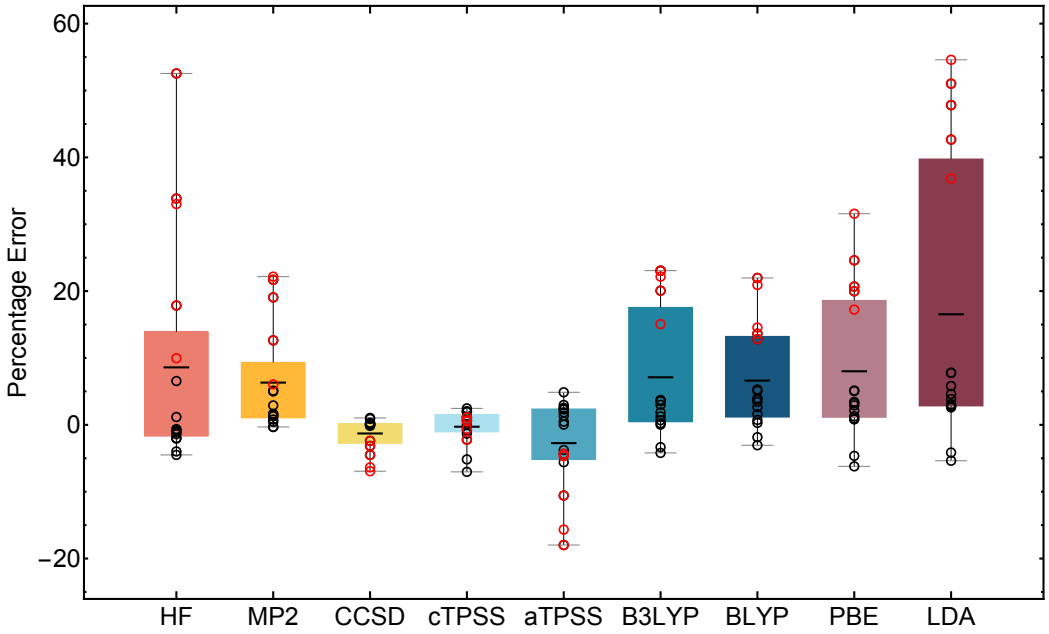

Figure 3. Box–whisker plot of the mean percentage error in the initial curvature $\xi_{xx} = \mathrm{d}^2E/\mathrm{d}B_x^2\big|_{\mathbf{B}=0}$ with the indicated method with unc-aug-cc-pVTZ basis set, relative to CCSD(T)/aug-cc-pCV5Z. The individual data points are shown as open circles; black circles correspond to the diamagnetic molecules and red to the paramagnetic molecules. Coloured boxes span the range between the 25% and 75% quantiles. The end fences of the whiskers correspond to the minimum and maximum errors for each functional considered. The mean percentage error is marked by a thick horizontal line.

well in magnetic fields—providing, for example, a good description of paramagnetic bonding in strong magnetic fields [5]. A good description of paramagnetic bonding depends on the ability of the model to describe the response of the electronic structure to the applied magnetic field. In closed-shell paramagnetic molecules, the paramagnetic response of the wave function is larger than in diamagnetic molecules and must be accurately described to obtain a reasonable accuracy in the calculated magnetizability. It is therefore tempting to speculate that the cTPSS functional provides a more reasonable description of the response of the electronic structure to the applied magnetic field in comparison with the other DFAs, but other factors may be important and we cannot exclude the possibility of a systematic error cancellation between dia- and paramagnetic contributions to the magnetizability.

5.3. *Field-dependence of the universal density functional*

We now consider the dependence of the BDFT density functional $F_\lambda(\rho, \mathbf{B})$ on the magnetic field $\mathbf{B}$ for a fixed density ρ. We examine first the simple situation where ρ is a v-representable density whose external potential v is such that the field-free Hamiltonian $H_\lambda(v, \mathbf{0})$ is rotationally symmetric about some axis. For simplicity, we align the z-axis of the coordinate system to this symmetry axis. For vanishing and parallel magnetic fields, the corresponding canonical angular-momentum component, $L_z = xp_y - yp_z$, is quantized and commutes with the Hamiltonian

$$[H_\lambda(v, \mathbf{0}), L_z] = 0. \tag{29}$$

If the ground state of $H_\lambda(v, \mathbf{0})$ is non-degenerate, it has vanishing angular momentum $m_z = \langle L_z \rangle = 0$. The same wave function is then ground state of $H_\lambda(v, \mathbf{0})$ and $H_\lambda(v - \frac{1}{2}A^2, \mathbf{A}) = H(v, \mathbf{0}) + \frac{1}{2}B_z L_z$ in some B_z-interval around zero field. If

the ground state is degenerate, the ground states at $B_z < 0$ and $B_z > 0$ are related by time reversal symmetry, their angular momenta m_z differing only by a sign. In both cases, the same density ρ is a ground-state density of $H_\lambda(v, \mathbf{0})$ and $H_\lambda(v - \frac{1}{2}A^2, \mathbf{A}) = H_\lambda(v, \mathbf{0}) + \frac{1}{2}B_z L_z$ in some B_z-interval around zero field. It follows that v and $v - \frac{1}{2}A^2$ are maximizing potentials in the Lieb variation principles for $F_\lambda(v, \mathbf{0})$ and $F_\lambda(v, \mathbf{B})$, respectively:

$$F_\lambda(\rho, \mathbf{0}) = \max_{v'} \big(E_\lambda(v', \mathbf{0}) - (v'|\rho)\big) = E_\lambda(v, \mathbf{0}) - (v|, \rho), \tag{30}$$

$$F_\lambda(\rho, \mathbf{B}) = \max_{v'} \big(E_\lambda(v', \mathbf{B}) - (v'|\rho)\big) = E_\lambda(v - \tfrac{1}{2}A^2, \mathbf{B}) - (v - \tfrac{1}{2}A^2|\rho). \tag{31}$$

Comparing Eqs. (30) and (31) and noting that $E_\lambda(v - \frac{1}{2}A^2, \mathbf{A}) = E_\lambda(v, \mathbf{0}) - \frac{1}{2}|B_z m_z|$, we arrive at the following simple expression for the field variation of the universal density functional for a fixed density:

$$\Delta F_\lambda(\rho, \mathbf{B}) = F_\lambda(\rho, \mathbf{B}) - F_\lambda(\rho, \mathbf{0}) = \tfrac{1}{2}(A^2|\rho) - \tfrac{1}{2}|B_z m_z|, \tag{32}$$

assuming that the potential v associated with ρ is such that the Hamiltonian commutes with the angular-momentum operator in the field direction. The field dependence consists of a simple quadratic diamagnetic term and a linear paramagnetic term. Note that we have the same dependence at all interaction strengths. These results are illustrated in Figure 4 for the beryllium and neon atoms.

Let us now consider the more general situation, with no conditions on the density. Performing the Kohn–Sham decomposition of the density functional, we obtain

$$F_\lambda(\rho, \mathbf{B}) = T_\mathrm{s}(\rho, \mathbf{B}) + \lambda J(\rho) + E_{\mathrm{xc},\lambda}(\rho, \mathbf{B}), \tag{33}$$

where the Hartree term does not depend explicitly on the field, yielding

$$\Delta F_\lambda(\rho, \mathbf{B}) = \Delta T_\mathrm{s}(\rho, \mathbf{B}) + \Delta E_{\mathrm{xc},\lambda}(\rho, \mathbf{B}). \tag{34}$$

In general, the field dependence of $F_\lambda(\rho, \mathbf{B})$ is dominated by the field dependence of the noninteracting kinetic energy, the exchange–correlation energy making a smaller contribution. We have not been able to calculate the field dependence of $F_1(\rho, \mathbf{B})$ for a fixed ρ directly, being unable to converge the Lieb maximization for the interacting systems for $\lambda > 0$. On the other hand, by solving the Lieb variation principle for $\lambda = 0$, we have been able to study the field dependence of the noninteracting kinetic energy and of the exchange energy (using Eq. (13)).

In Figure 5, we have plotted $E_\mathrm{x}(\rho, \mathbf{B})$ for a selection of atoms and molecules evaluated as a function of the field strength for the field-free ground-state density. For He, Be, and Ne, the exchange energy is unaffected by the magnetic field since the wave function remains fixed, for reasons discussed earlier. The H_2 molecule is a single-orbital system with $E_\mathrm{x}(\rho, \mathbf{B}) = -\frac{1}{2}J(\rho)$, again leading to an unaffected exchange energy. We observe that, also for LiH and H_2O, the exchange-energy remains essentially constant up to $0.03B_0$. In contrast, benzene and pyrrole show a more pronounced, though still small field dependence. For these systems $E_\mathrm{x}(\rho, \mathbf{B})$ increases as the perpendicular field strength increases. The paramagnetic molecules show a much stronger dependence of $E_\mathrm{x}(\rho, \mathbf{B})$ on the applied field, exhibiting a decreasing quadratic behaviour in the exchange, opposite to that for benzene and pyrrole.

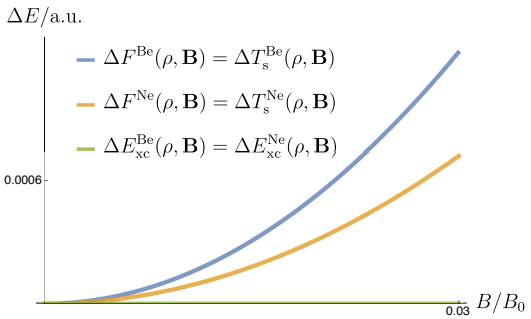

Figure 4. BDFT density functional and its Kohn–Sham energy components relative to the zero-field values as a function of the magnetic field strength for Ne and Be. All functionals were evaluated at the zero-field ground-state density at the CCSD level using the unc-aug-cc-pVTZ basis set.

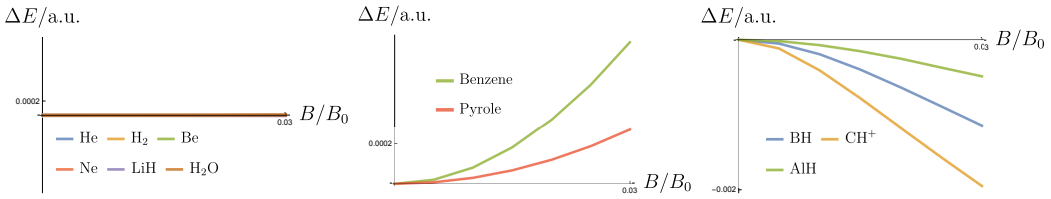

Figure 5. BDFT exchange energy relative to the zero-field values as a function of the magnetic field strength. All calculations have been carried out at fixed zero-field density, with an uncontracted cc-pVTZ basis for benzene and pyrrole and the unc-aug-cc-pVTZ basis for the other molecules. For AlH, benzene and pyrrole, the calculations have been performed at the MP2 level, whereas, for the remaining molecules, calculations have been performed at the CCSD level.

6. Conclusions

Within the framework of BDFT, we have examined the field dependence of the total energy and its Kohn–Sham components as a function of the magnetic field strength for a number of popular DFAs at the GGA, meta-GGA and hybrid levels of theory. For diamagnetic molecules, the field dependence of the total energy and the Kohn–Sham components is modelled well by all functionals, even those that neglect the field dependence of the exchange–correlation functional altogether. The reason for this good behaviour is that the electronic structure of diamagnetic molecules is only weakly perturbed by an applied magnetic field. By contrast, the electronic structure of closed-shell paramagnetic molecules is strongly affected by an applied magnetic field, making their accurate description more difficult. For such molecules, the performance is in general poorer, also for the HF, MP2, and CCSD wave-function methods. Nevertheless, the paramagnetic molecules are correctly identified by all methods considered here. Moreover, all DFAs provide a qualitatively correct field dependence of the Kohn–Sham components also for these difficult systems. The performance of the cTPSS functional is impressive: It performs equally well for dia- and paramagnetic molecules, outperforming MP2 theory for the closed-shell paramagnetic molecules considered here. At present, the reason for the good performance of the cTPSS functional is not known and it may arise from error cancellation. We note however, that we have also previously observed that it performs well in magnetic fields—providing, for example, a good description of paramagnetic bonding in strong magnetic fields [5].

In BDFT, the performance of a DFA in a magnetic field is determined both by the density dependence and the field dependence of the exchange–correlation functional. We have therefore also studied $F_\lambda(\rho, \mathbf{B})$ as a function of $\mathbf{B}$ for a fixed density ρ. For atoms, where the Hamiltonian commutes with the angular-momentum operator in

the field direction, the exchange–correlation energy is unaffected by the magnetic field. For other systems, indications are that the field dependence is small. Even for closed-shell paramagnetic molecules, paramagnetism is driven by kinetic energy, with a much smaller contribution from the exchange–correlation functional.

7. Acknowledgements

This work was supported by the Research Council of Norway through its Centres of Excellence scheme, project number 262695 and through the European Research Council under the European Union Seventh Framework Program through the Advanced Grant ABACUS, ERC Grant Agreement No. 267683. EIT was supported by the Norwegian Research Council through Grant No. 240674. AMT is grateful for support from a Royal Society University Research Fellowship and the Engineering and Physical Sciences Research Council EPSRC, Grant No. EP/M029131/1. S. S. acknowledges support by the Deutsche Forschungsgemeinschaft (Grant No. DFG STO 1239/1-1). The authors are grateful to the the Centre for Advanced Study at the Norwegian Academy of Science and Letters, Oslo, Norway, where a substantial part of this work was carried out under the project Molecules in Extreme Environments.

References

[1] N. Maridrossian and M. Head-Gordon, Mol. Phys. **115**, 2315 (2017).
[2] G. Vignale and M. Rasolt, Phys. Rev. Lett. **59**, 2360 (1987).
[3] G. Vignale and M. Rasolt, Phys. Rev. B **37**, 10685 (1988).
[4] E.I. Tellgren, S. Kvaal, E. Sagvolden, U. Ekström, A.M. Teale and T. Helgaker, Phys. Rev. A **86**, 062506 (2012).
[5] J.W. Furness, J. Verbeke, E.I. Tellgren, S. Stopkowicz, U. Ekström, T. Helgaker and A.M. Teale, J. Chem. Theory Comput. **11** (9), 4169 (2015).
[6] C.J. Grayce and R.A. Harris, Phys. Rev. A **50**, 3089 (1994).
[7] S. Reimann, A. Borgoo, E.I. Tellgren, A.M. Teale and T. Helgaker, J. Chem. Theory Comput. **13** (9), 4089 (2017).
[8] E.I. Tellgren, Phys. Rev. A **97**, 012504 (2018).
[9] K.K. Lange, E.I. Tellgren, M.R. Hoffmann and T. Helgaker, Science **337** (6092), 327 (2012).
[10] S. Stopkowicz, J. Gauss, K.K. Lange, E.I. Tellgren and T. Helgaker, J. Chem. Phys. **143**, 074110 (2015).
[11] S. Stopkowicz, Implementation of relaxed coupled cluster doubles densities for molecules in magnetic fields 2017, personal communication.
[12] J. Austad, Second-order Møller–Plesset perturbation theory in strong magnetic fields 2018, in preparation.
[13] S. Stopkowicz, Molecular gradients at the coupled-cluster level for atoms in molecules in strong magnetic fields 2018, in preparation (2018).
[14] E.H. Lieb, Int. J. Quantum Chem. **24**, 243 (1983).
[15] G. Vignale, M. Rasolt and D.J.W. Geldart, Phys. Rev. B **37**, 2502 (1988).
[16] S.M. Colwell and N.C. Handy, Chem. Phys. Lett. **217** (3), 271 (1994).
[17] A.M. Lee, N.C. Handy and S.M. Colwell, J. Chem. Phys. **103** (23), 10095 (1995).
[18] E.I. Tellgren, A.M. Teale, J.W. Furness, K.K. Lange, U. Ekström and T. Helgaker, J. Chem. Phys. **140** (3), 034101 (2014).
[19] S.N. Maximoff and G.E. Scuseria, Chem. Phys. Lett. **390** (4-6), 408 (2004).
[20] J.F. Dobson, J. Chem. Phys. **98**, 8870 (1993).
[21] E. Sagvolden, U. Ekström and E. Tellgren, Mol. Phys. **111**, 1295 (2013).
[22] J.E. Bates and F. Furche, J. Chem. Phys. **137** (16), 164105 (2012).
[23] W. Zhu, L. Zhang and S.B. Trickey, Phys. Rev. A **90**, 022504 (2014).
[24] J.D. Talman and W.F. Shadwick, Phys. Rev. A **14**, 36 (1976).
[25] T. Heaton-Burgess, P. Ayers and W. Yang, Phys. Rev. Lett. **98**, 036403 (2007).
[26] F. Neumann, R.H. Nobes and N.C. Handy, Mol. Phys. **87**, 1 (1996).
[27] P.W. Fowler and E. Steiner, Mol. Phys. **74**, 1147 (1991).

[28] S.P.A. Sauer, T. Enevoldsen and J. Oddershede, J. Chem. Phys. **98**, 9748 (1993).
[29] O.B. Lutnæs, A.M. Teale, T. Helgaker, D.J. Tozer, K. Ruud and J. Gauss, J. Chem. Phys. **131**, 144104 (2009).
[30] A.M. Teale, O.B. Lutnæs, T. Helgaker, D.J. Tozer and J. Gauss, J. Chem. Phys. **138** (2), 024111 (2013).
[31] K. Ruud, T. Helgaker, K.L. Bak, P. Jørgensen and J. Olsen, Chem. Phys. **195** (1), 157 (1995).
[32] A. Mellouki, J. Liévin and M. Herman, Chem. Phys. **271** (3), 239 (2001).
[33] W. Zhu and S.B. Trickey, The Journal of Chemical Physics **147** (24), 244108 (2017).
[34] CFOUR, a quantum chemical program package written by J.F. Stanton, J. Gauss, M.E. Harding, P.G. Szalay with contributions from A.A. Auer, R.J. Bartlett, U. Benedikt, C. Berger, D.E. Bernholdt, Y.J. Bomble, L. Cheng, O. Christiansen, M. Heckert, O. Heun, C. Huber, T.-C. Jagau, D. Jonsson, J. Jusélius, K. Klein, W.J. Lauderdale, D.A. Matthews, T. Metzroth, L.A. Mück, D.P. O'Neill, D.R. Price, E. Prochnow, C. Puzzarini, K. Ruud, F. Schiffmann, W. Schwalbach, C. Simmons, S. Stopkowicz, A. Tajti, J. Vázquez, F. Wang, J.D. Watts and the integral packages MOLECULE (J. Almlöf and P.R. Taylor), PROPS (P.R. Taylor), ABACUS (T. Helgaker, H.J. Aa. Jensen, P. Jørgensen, and J. Olsen), and ECP routines by A. V. Mitin and C. van Wüllen. For the current version, see http://www.cfour.de. 2016.
[35] J. Gauss, K. Ruud and M. Kállay, J. Chem. Phys. **127** (7), 074101 (2007).
[36] QUEST, a rapid development platform for QUantum Electronic Structure Techniques, http://quest.codes .
[37] E.I. Tellgren, A. Soncini and T. Helgaker, J. Chem. Phys. **129** (15), 154114 (2008).
[38] LONDON, a quantum-chemistry program for plane-wave/GTO hybrid basis sets and finite magnetic field calculations. By E. Tellgren (primary author), T. Helgaker, A. Soncini, K. K. Lange, A. M. Teale, U. Ekström, S. Stopkowicz, J. H. Austad, and S. Sen. See londonprogram.org for more information. .
[39] F. London, J. Phys. Radium **8** (10), 397 (1937).
[40] T.H. Dunning, J. Chem. Phys. **90** (2), 1007 (1989).
[41] D.E. Woon and T.H. Dunning, J. Chem. Phys. **100** (4), 2975 (1994).
[42] Q. Wu and W. Yang, J. Chem. Phys. **118** (6), 2498 (2003).
[43] A.M. Teale, S. Coriani and T. Helgaker, J. Chem. Phys. **130**, 104111 (2009).
[44] E.I. Tellgren, T. Helgaker and A. Soncini, Phys. Chem. Chem. Phys. **11**, 5489 (2009).
[45] S. Loibl and M. Schütz, J. Chem. Phys. **141**, 024108 (2014).